STUDY ON THE BEHAVIOR OF SUSPENDED SOLIDS IN THE NERITIC REGION IN AN INNER BAY

HIROAKI TANAKA
Saga University, Graduate School of Science and Engineering, Saga, Japan, 19709004@edu.cc.saga-u.ac.jp

HIDEO OSHIKAWA
Saga University, Saga, Japan, oshikawa@cc.saga-u.ac.jp

AKIRA TAI
Kyushu University, Fukuoka, Japan, tai@civil.kyushu-u.ac.jp

YUICHI HAYAMI
Saga University, Saga, Japan, hayami@cc.saga-u.ac.jp

ABSTRACT

In recent years, the behavior of suspended solids (SS) in coastal areas has been investigated. However, because SS consist mostly of fine cohesive particles, their physical and chemical characteristics have not been sufficiently determined. In this study, in order to clarify the properties of SS in the neritic region in an inner bay, the effects of sea surface waves, currents, and turbulence on SS were investigated by conducting field observations in Isahaya Bay in the Ariake Sea, which is a typical enclosed sea and has the largest tidal range in Japan. Turbidity was used for the analysis as a proxy for SS because it is difficult to measure SS continuously. Spectral analysis of flow velocity, water pressure near the sea bottom, and water depth were carried out to reveal fluctuations in turbidity. The results showed that wind waves and related wave breaking were important for increasing turbidity and that the anisotropy of turbulence was strengthened by the wave breaking. Therefore, both wind waves and wave breaking should be considered adequately in the evaluation and prediction of the behavior of SS in inner bays.

Keywords: Turbidity, wave, tidal current, turbulence, wave breaking

1. INTRODUCTION

The behavior of suspended solids (SS) in coastal areas has been a recent research focus (Winterwarp et al., 2012). However, the physical and chemical characteristics of SS are not well understood because SS consist mainly of fine cohesive particles.

The Ariake Sea, in the northwest of Kyushu Island, Japan, is the largest inner bay in Kyushu Island. The sea is enclosed by Fukuoka, Kumamoto, Saga, and Nagasaki prefectures (Figure 1). The tidal range of the Ariake Sea is larger than 5 m at the end of the sea during spring tides, and the sea is an important macrotidal estuary with the largest tidal flat in Japan. A water area reclamation project was started in 1990 in the Isahaya Bay in the Ariake Sea, and the end of the bay has

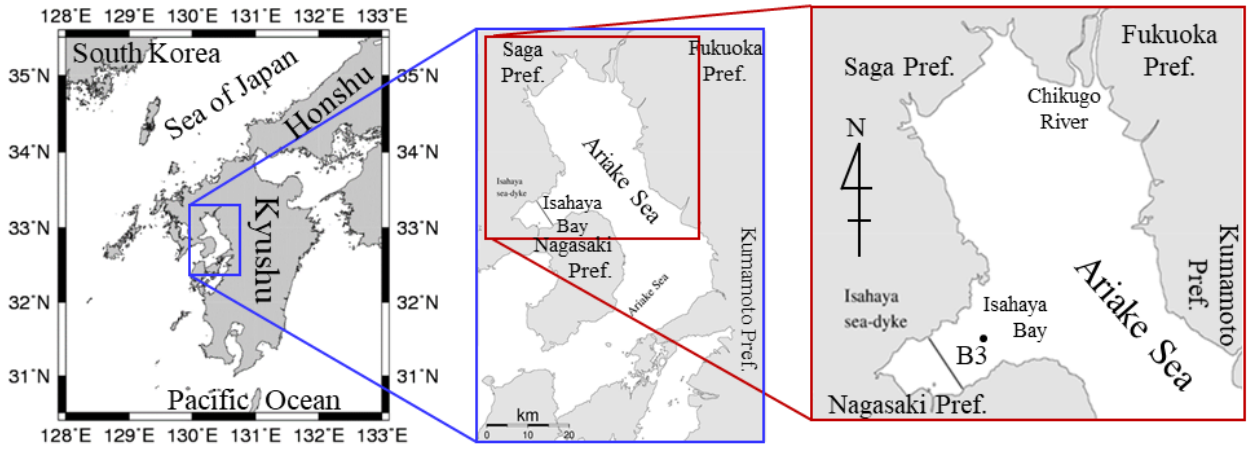

Figure 1. Location of the Ariake Sea, Isahaya Bay, and the observation point.

been closed since 1997 owing to the construction of the Isahaya sea-dyke (Picture 1(a)). The project may have changed the flow structure of the Ariake Sea and decreased its water quality (Tai et al., 2013).

Flow structures in Isahaya Bay and the surrounding region have been measured. Nakamura et al. (2003) measured flow velocity with an acoustic Doppler current profiler (ADCP) in a depression below sea level at the mouth of Isahaya Bay in 2002 and reported the tidal current ellipse and vertical flow structure of the residual current. Additionally, Yano et al. (2005) compared the tidal current before and after the construction of the Isahaya sea-dyke and demonstrated that the principal lunar semidiurnal component (M2) decreased in some parts of the Ariake Sea.

Li and Matsunaga (2010) investigated the bottom sediment environment in Isahaya Bay and reported that the grain size of the bottom sediment had decreased. Furthermore, Nakagawa et al. (2002, 2007, 2009) took in situ measurements in the northern Ariake Sea and the eastern Ariake Sea off the port of Kumamoto, and investigated the response characteristics of the bottom sediment. They showed that the mean flow velocity obtained with an ADCP was not sufficient to estimate the external force on sediment transport, and also found that fluctuating components, including wind waves, were important for sediment transport. However, there are insufficient field survey studies on the characteristics of bottom sediment transport in Isahaya Bay, and the mechanism of the grain size refining reported by Li and Matsunaga (2010) is not sufficiently understood.

Since 2013, our research group has conducted field observations in Isahaya Bay for approximately two months in every winter and summer (e.g., Tai et al., 2015). Oshikawa et al. (2016) examined the response characteristics of turbidity in the bay depending on flow velocities, turbulence, and waves via a multiple regression analysis. However, that study did not reveal these response characteristics sufficiently. Therefore, in the present study, the data obtained by Oshikawa et al. (2016) were subjected to additional analysis, and subsequent field observation data were also analyzed and discussed, with a particular focus on wave breaking.

2. FIELD OBSERVATIONS

In order to estimate the response characteristics of SS and bottom sediment in Isahaya Bay, long-term field measurements were conducted close to an observation tower (Station B3, Figure 1 and Picture 1(b)) managed by the Kyushu Regional Agricultural Administration Office. Observations were performed in winter from 22 December 2013 to 2 March 2014 (fiscal year [FY] 2013) and in winter from 22 February to 29 March 2016.

(a) The Isahaya sea dyke.

(b) Observation tower.

Picture 1. Photos taken from the observation point.

The instruments used for the analysis and their properties are listed in Tables 1 and 2. In the Wave Hunter 04-Σ (I.O. Technic Co., Ltd.), water surface elevation and each horizontal velocity component were simultaneously measured by a pressure-type wave gage, an ultrasonic-type wave gage, and an electromagnetic current meter. Additionally, water surface elevation and each of the three components of flow velocity were simultaneously measured by a pressure-type wave gage and an ultrasonic-type current meter with the VECTOR (Nortek As). Each measured height given in Tables 1 and 2 is the length between the sea bottom and the sensor head, which was measured immediately after the installation of the instruments.

Mean water depth was measured using the ultrasonic-type wave gage because the measurement accuracy of this type of wave gage is generally higher than that of pressure-type wave gages. The average value of water depth with a simple correction in the case with wave-breaking was 8.6 m in FY 2013 and 8.4 m in 2016. Therefore, the long-term mean water depth (h_m) was taken as the mean value of these two values, that is, 8.5 m.

Furthermore, grain size distributions were measured. Surface sediment was sampled immediately before the installation and the removal of the measuring instruments. The median grain size of the surface sediment (d_{50}) was an average of 29 μm.

Table 1. Measuring instruments and conditions (winter FY 2013).

Observed items	Measuring instruments	Measured height	Burst time and Sampling frequency
Flow velocity and Water level	Ultrasonic-type current meter with a pressure-type wave gage (Nortek As, VECTOR)	25 cm	Every 2 hours, 128 sec at 32 Hz
Water level and Pressure	Wave gages with an electromagnetic current meter (IOTechnic, Wave Hunter04-Σ)	50 cm	Every 1 hour, 1200 sec at 5 Hz
Turbidity and Chlorophyll concentration	Turbidimeter (JFE Advantech, Compact-CLW)	35 cm	Every 30 min, 30 sec at 2 Hz

Table 2. Measuring instruments and conditions (winter 2016).

Observed items	Measuring instruments	Measured height	Burst time and Sampling frequency
Flow velocity and Water level	Ultrasonic-type current meter with a pressure-type wave gage (Nortek As, VECTOR)	30 cm	Every 2 hours, 256 sec at 16 Hz
Water level and Pressure	Wave gages with an electromagnetic current meter (IOTechnic, Wave Hunter04-Σ)	55 cm	Every 1 hour, 1200 sec at 5 Hz
Turbidity and Chlorophyll concentration	Turbidimeter (JFE Advantech, Compact-CLW)	30 cm	Every 30 min, 30 sec at 2 Hz

3. Long-term variation of measured physical quantities

Figure 2 shows representative long-term measured data of significant wave height ($H_{1/3}$), significant wave period ($T_{1/3}$), mean water depth measured by a pressure-type wave gage attached to Wave Hunter for 20 min (*WL*), a time variation of *WL* calculated by the finite difference method (corresponding to the magnitude of the tidal current) (*dWL/dt*), turbulence energy measured by VECTOR (*k*), and turbidity. Turbulence energy is expressed by Eq. (1).

$$k = \frac{1}{2}\left(\langle u'^2 \rangle + \langle v'^2 \rangle + \langle w'^2 \rangle\right) \tag{1}$$

where *u*, *v*, and *w* are the instantaneous velocities for the north-south, east-west, and vertical components, respectively; *u'* (= *u* - <*u*>), *v'* (= *v* - <*v*>), *w'* (= *w* - <*w*>) are fluctuations of each mean velocity component (<*u*>, <*v*>, <*w*>); and angular

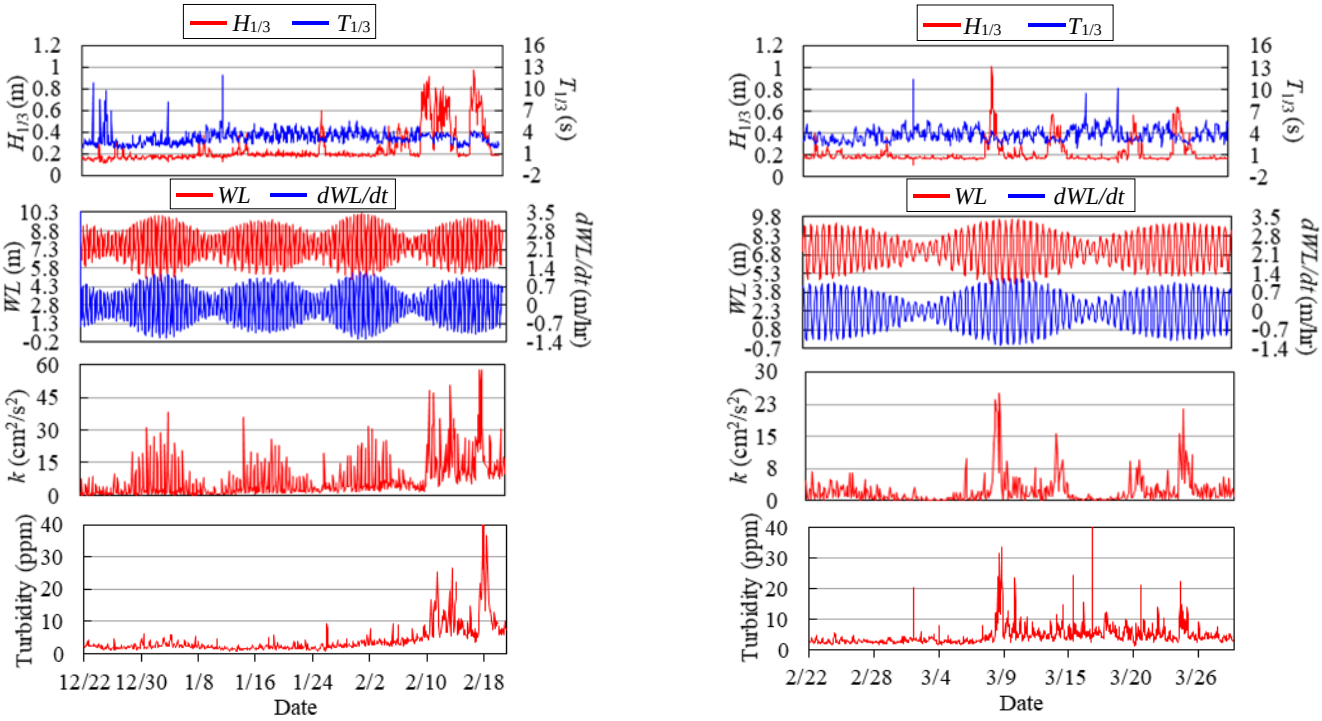

(a) FY 2013. (b) 2016.

Figure 2. Temporal variations of the averaged measurements.

brackets represent time averaging. Turbidity was calibrated as SS with data for kaolin from JFE Advantech Co., Ltd., and the 1 h moving average was calculated.

As shown in Figure 2(a), both $H_{1/3}$ and turbidity were high in mid-February in the winter of FY 2013. While in Figure 2(b), both $H_{1/3}$ and turbidity increased on 9, 14, 21, and 24 March in winter 2016. Additionally, Figure 2 demonstrates that k was related to WL and dWL/dt since k was large in the spring tides.

Based on the data shown in Figure 2, two events were selected in which the effects of k, WL, dWL/dt, or mean velocity near the seabed (V_{bm}) on turbidity were remarkable. One of these occurred around 11 February 2014, when k, $H_{1/3}$, and turbidity increased (Figure 2(a)); hereafter, this is referred to as Event A. Oshikawa et al. (2016) already discussed the event on 18 February 2014, which had the largest turbidity, wave height and turbulent energy, but did not focus on the event around 11 February 2014. Event A is discussed in Section 4. Additionally, as shown in Figure 2(b), both turbidity and $H_{1/3}$ were especially large around 9 March 2016, and this increase is hereafter referred to as Event B. The effects of tidal current in Event B should be large compared with those in Event A, as 9 March 2016 corresponded to a spring tide, as shown in Figure 2(b). Event B is discussed in Section 5.

4. DISCUSSION OF THE EVENT AROUND 11 FEBRUARY 2014 (EVENT A)

In this section, in order to reveal the factors that caused k, $H_{1/3}$, and turbidity to be especially large at around 17:00 local time on 11 February 2014 (Figure 2(a)), two time series of data, which are defined as Burst 1 and Burst 2, respectively, are selected and compared. Burst 2 is the time series data set from 17:00 on 11 February 2014, and Burst 1 is that from 17:00 on 10 February 2014, that is, 24 h before Burst 2.

The effects of the tidal current on turbidity should be small at around 11 February 2014, which corresponded to a transitional tide between the spring and neap tides, as shown in Figure 2(a). However, Oshikawa et al. (2016) reported that the tidal current contributed to increasing turbidity on 18 February 2014. The tidal conditions, including tidal current, should be almost the same in Burst 1 and Burst 2 as the time difference of 24 h is short relative to the time difference between spring tides.

Wave breaking was observed in Burst 2. Figure 3 shows the time series instantaneous pressure head near the seabed (p) and water depth (η) which were measured by Wave Hunter. The values of $H_{1/3}$, as measured by the pressure-type wave gage, are 0.73 m and 0.92 m in Burst 1 and Burst 2, respectively. Consequently, the sea surface waves were higher in Burst 2 than in Burst 1. As shown in Figure 3(a), in Burst 1, p and η has almost the same fluctuations with a cycle of 3.8 s. However, as shown in Figure 3(b), in Burst 2, the fluctuations of p and η are different, most remarkably at around 1080 s. Therefore, the difference between p and η in Burst 2 depends on wave breaking because the reason why whitecaps generated by wave breaking deteriorated the measurement accuracy of the water surface with the ultrasonic-type wave gage. In particular, spilling breakers must have occurred in Burst 2 as the mean water depth was too large for shallow water waves to exist.

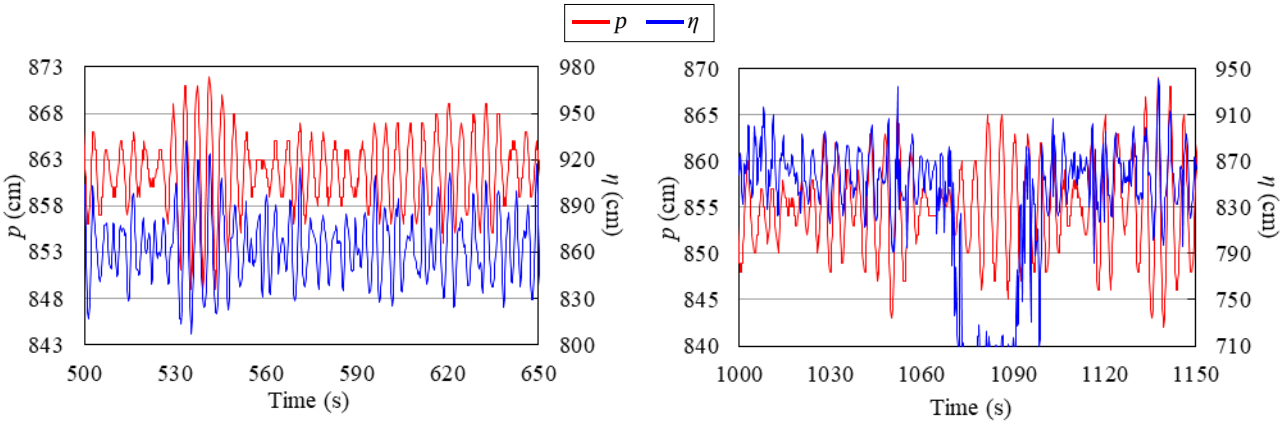

(a) Burst 1 (17:00 on 10 Feb).

(b) Burst 2 (17:00 on 11 Feb).

Figure 3. Instantaneous pressure head and water level in Februay 2014.

The time series of each instantaneous velocity component and pressure head in Burst 2 measured by VECTOR are shown in Figure 4. A high wave grouping with a period of about 4 s was observed, and turbulence was superimposed on this grouping (Goda, 2008).

Figure 5 shows the frequency spectra of Burst 1 and Burst 2 calculated from time series data in Figures 3 and 4 via fast Fourier transform. f is the frequency and $F_u(f)$, $F_v(f)$, and $F_w(f)$ are frequency spectra for each velocity component (u, v, w), respectively. $F_\eta(f)$ is the frequency spectrum for water surface elevation obtained from the ultrasonic-type wave gage, and $F_p(f)$ is the frequency spectrum for water pressure obtained from the pressure-type wave gage equipped on Wave

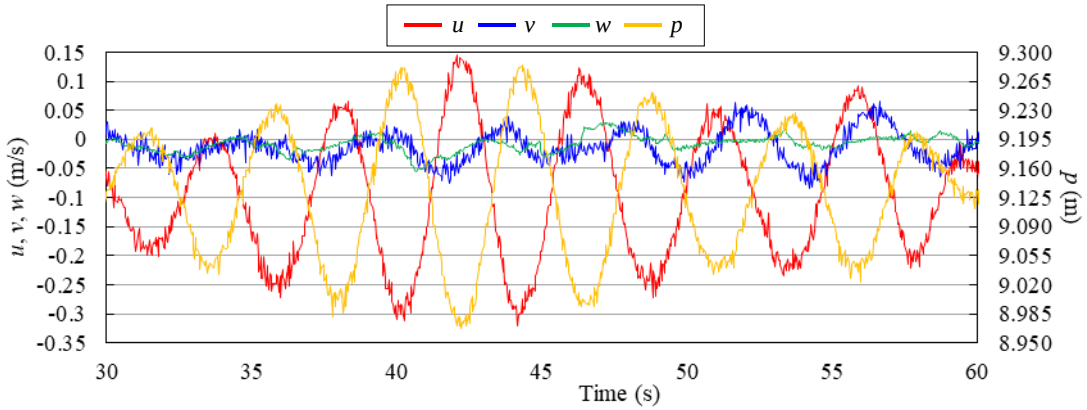

Figure 4. Raw data for each velocity component and pressure head in Burst 2 in 17:00, 11 February 2014.

Hunter. Figure 5(c) shows the velocity spectra of pure turbulence because the dominant components of sea surface waves are removed from Figure 5(b) as discussed in detail below.

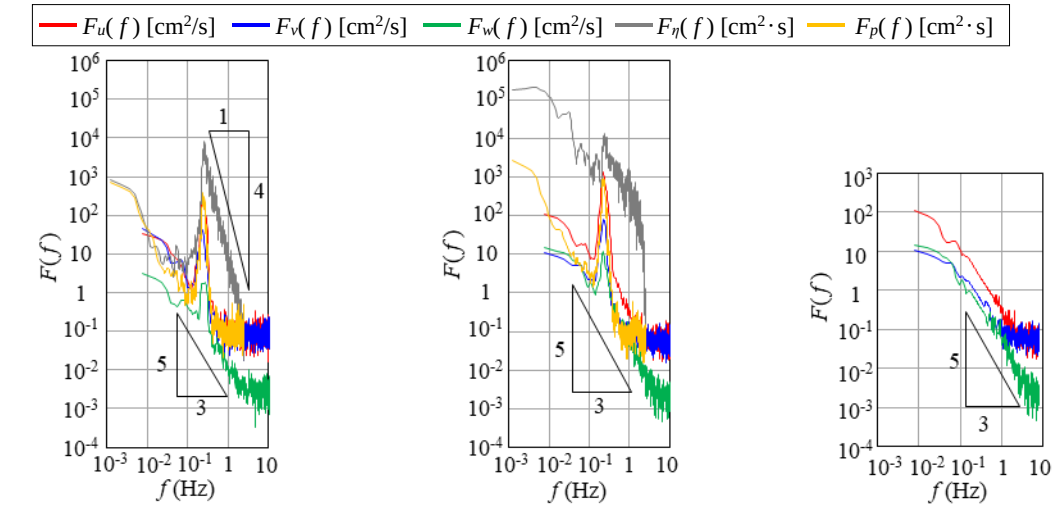

(a) Burst 1 (17:00, 10 Feb). (b) Burst 2 (17:00, 11 Feb). (c) Burst 2.

Figure 5. Frequency spectra of velocities near the seabed and waves in February 2014.

As shown in Figure 5(a) in Burst 1, the peak in $F_\eta(f)$ was observed at a frequency of 0.26 Hz, and a double logarithmic plot of $F_\eta(f)$ followed the –4 power law for wind surface waves (Mitsuyasu, 1995). Additionally, the velocity spectra in Figure 5(a) have peaks at the frequency of 0.26 Hz, indicating that the motion of sea surface waves extended to the velocity fluctuation near the seabed. Moreover, Figure 5(a) shows that the inertial subranges of turbulence followed the –5/3 power law except near the peaks.

On the other hand, as shown in Figure 5(b), in Burst 2, the double logarithmic plot of $F_\eta(f)$ did not follow the –4 power law, and at low frequencies $F_\eta(f)$ is much larger than that in Figure 5(a) due to wave breaking. Wind waves should be fully developed not only in Burst 1 but also in Burst 2 since the $F_p(f)$ in Burst 2 is larger than that in Burst 1 at almost all frequencies. Note that the pressure-type wave gage detected sea surface waves even if these included wave breaking, as shown in Figure 3(b). The wave height in Burst 2 should be significantly larger than that in Burst 1 because the peak in $F_p(f)$ is remarkably larger in Figure 5(b) than in Figure 5(a).

The magnitude of turbulence was larger in Burst 2 than in Burst 1 since the $F(f)$ of the inertial subranges of turbulence is generally larger in Burst 2 than in Burst 1. Because sea surface wave components were superimposed on turbulence in locations where wind waves developed, the turbulence statistics were recalculated using the inverse Fourier transform in order to eliminate the effect of wind waves from the time series data, in which the Fourier spectrum near the peak frequency was replaced by the –5/3 power law as follows:

$$F(f) = \alpha f^{-5/3} \tag{2}$$

where each constant α was manually determined in order to match the measured $F_u(f)$, $F_v(f)$, and $F_w(f)$ using Eq. (2), respectively, except for their peaks. Figure 5(c) shows the velocity spectra of each component of the recalculated results. As shown in the figure, there was no peak frequency, and the inertial subrange for turbulence had a wide frequency range in each spectrum.

In Figure 5(c), $F_u(f)$ is markedly larger than $F_v(f)$ and $F_w(f)$ in almost all frequency ranges ($f \leq 2.3$ Hz) as a parallel translation, which is obvious when Burst 2 in Figure 5(c) is compared with Burst 1 in Figure 5(a). The anisotropy of horizontal turbulent flow including spilling breakers is remarkable.

Additionally, the mean wave directions in Burst 1 and Burst 2 were calculated using Eq. (3), below (Goda, 1981), with the data measured by VECTOR, because wind waves were fully developed in both bursts.

$$\theta = \tan^{-1}\{(-\langle p'u' \rangle)/(-\langle p'v' \rangle)\} \tag{3}$$

where the angle of waves from the east was set as 0 and p' (= p - <p>) is a fluctuation from the mean pressure head <p>. Because θ equals 87° in Burst 1 and 92° in Burst 2, waves are southward in both bursts since north-south fluctuations are dominant, as shown in Figure 4.

The anisotropy of turbulence was confirmed with each component of turbulence intensity in Burst 1 and Burst 2 without coordinate transformation because both of the mean wave directions are nearly equal to 90°. Turbulence intensity was calculated using the data measured by VECTOR. Each component is as follows: $<(u')^2>^{1/2}$ =1.58 cm/s, $<(v')^2>^{1/2}$ = 1.56 cm/s, and $<(w')^2>^{1/2}$ = 0.46 cm/s in Burst 1, and $<(u')^2>^{1/2}$ =2.54 cm/s, $<(v')^2>^{1/2}$ = 1.22 cm/s, and $<(w')^2>^{1/2}$ = 1.03 cm/s in Burst 2. Note that each turbulence intensity was calculated by using the data after eliminating dominant wave components using the Fourier inverse transformation of the data shown in Figure 5(c). The turbulence anisotropy was much higher in Burst 2 than in Burst 1 because the rate of horizontal turbulence intensity, $<(u')^2>^{1/2}/<(v')^2>^{1/2}$, was 2.1 in Burst 2 while it was 1.0 (meaning horizontally isotropic turbulence) in Burst 1. Vertical turbulence intensity was relatively small compared with horizontal turbulence intensity since the mean water depth is much smaller than the horizontal length scale of the Ariake Sea or the Isahaya Bay.

The turbidity was higher in Burst 2 than in Burst 1 due to the increase of wave height and the wave breaking. The relationships among turbidity, mean flow velocity, wave height, and turbulence were examined. Turbidity, WL, V_{bm}, $H_{1/3}$, k, the turbulence energy without sea surface wave components based on the calculation of Figure 5(c) (k^*), and dWL/dt were found to be 5.2 ppm, 8.41 m, 5.5 cm/s, 0.73 m, 12 cm^2/s^2, 2.6 cm^2/s^2, and 0.34 m/hr, respectively, in Burst 1, and 14.1 ppm, 8.28 m, 8.0 cm/s, 0.92 m, 47 cm^2/s^2, 4.5 cm^2/s^2, and 0.57 m/hr, respectively, in Burst 2. That is, in Burst 1, the turbidity is relatively small even though waves are dominant, because $|dWL/dt|$, which corresponds to the magnitude of the tidal current, is relatively small (see Figure 2(a)). On the other hand, in Burst 2, the turbidity is relatively large since wave height and turbulence are markedly large. It is considered that, in Burst 2, the turbulent components of u were amplified due to wave breaking, and thus turbulence developed further, so that the turbidity was higher in Burst 2 than in Burst 1.

5. DISCUSSION OF THE EVENT ON 9 MARCH 2016 (EVENT B)

In order to reveal the factors that cause both turbidity and $H_{1/3}$ to be large on 9 March 2016, as shown in Figure 2(b), three time series of data were selected and compared in this section. These three time series were from around 0:00, 10:00, and 12:00 o'clock local time on 9 March 2016, and are referred to as Burst 3, Burst 4, and Burst 5, respectively. The time difference between Burst 3 and Burst 5 (12 hours) corresponds to the period of the principal lunar semidiurnal component, which is a dominant tidal component in the Ariake Sea (Yano et al., 2005).

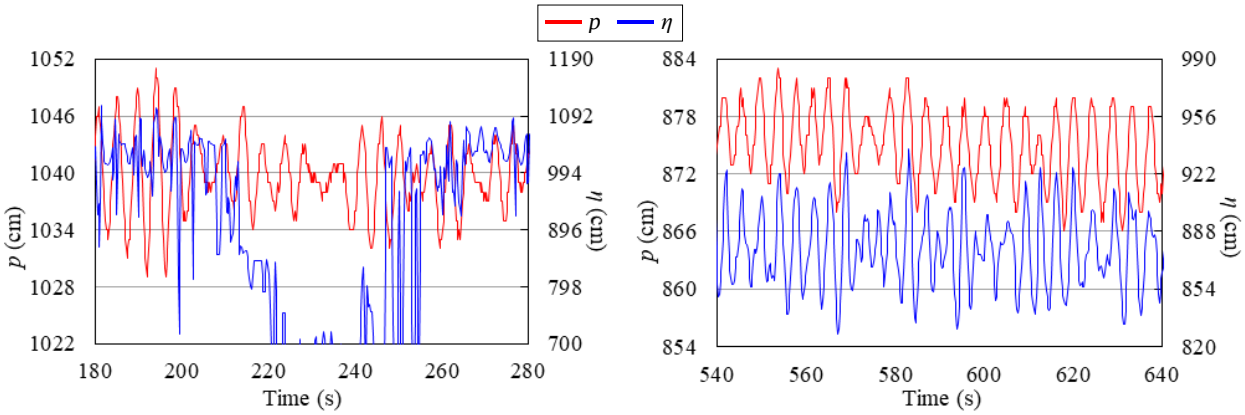

(a) Burst 4 (10:00). (b) Burst 5 (12:00).

Figure 6. Instantaneous pressure head and water level in 9 March 2016.

The time series of p and η measured by Wave Hunter for Burst 4 and Burst 5 are shown in Figure 6(a) and 6(b), respectively. As shown in the figure, a spilling breaker also appeared in Burst 4. As shown in Figure 6(b), in Burst 5, p and η had almost same fluctuations, with a cycle of 4.2 s. However, as shown in Figure 6(a), in Burst 4, the fluctuations of p and η are different, most remarkably at around 230 s. The wave height was larger in Burst 4 than in Burst 5 with the

$H_{1/3}$ measured by the pressure-type wave gage being 0.61 m for Burst 5 and 0.89 m for Burst 4. Therefore, in Burst 4, the difference between p and η depends on wave breaking, as discussed with Figure 3(b).

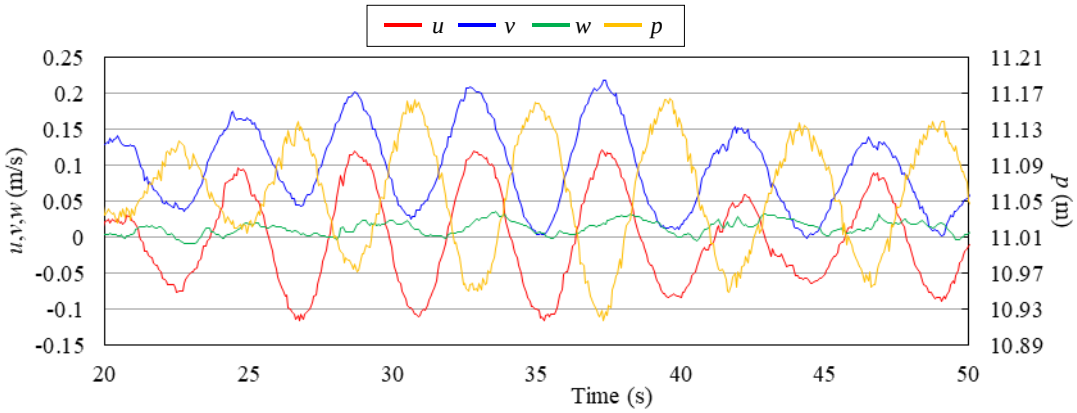

Figure 7. Raw data for each velocity component and pressure head in Burst 4 on 9 March 2016.

Figure 7 shows the time series of each instantaneous velocity component and pressure head in Burst 4 measured by VECTOR. Waves with a period of about 4.4 s were observed. Eastward mean flow velocity is remarkable since <u>, <v>, and <w> are 0.002 m/s, 0.108 m/s, and 0.014 m/s, respectively. Therefore, the mean flow velocity of Burst 4 is considerably large as seen from the value of 0.108 m/s in <v>, although Burst 4 corresponds to a high tide as explained later and tidal current should be nearly zero.

Figure 8 shows the frequency spectra of bursts 3, 4, and 5 calculated from the time series data in Figures 6 and 7.

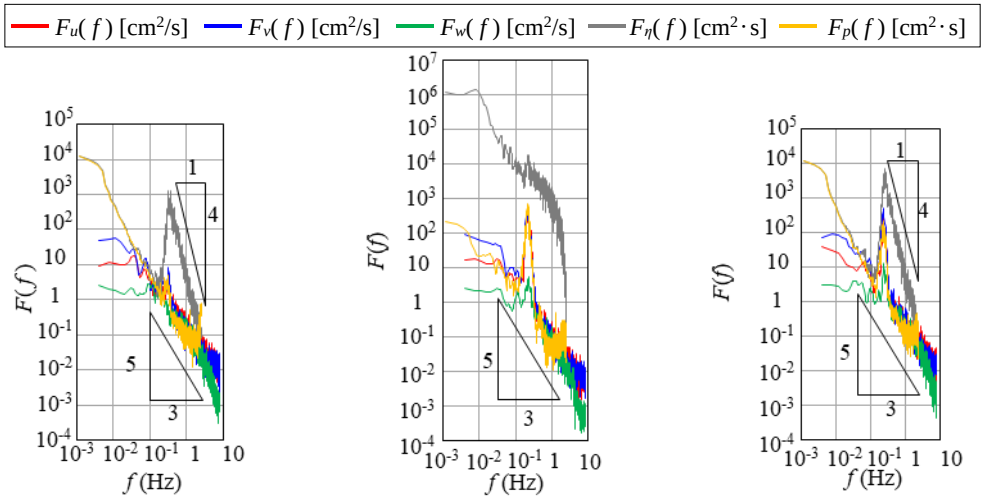

(a) Burst 3 (0:00). (b) Burst 4 (10:00). (c) Burst 5 (12:00).

Figure 8. Frequency spectra of velocities near the seabed and waves for three bursts on 9 March 2016.

As shown in Figure 8(c), in Burst 5, the peaks were observed at the same frequency of 0.24 Hz in each spectrum and a double logarithmic plot of $F_\eta(f)$ followed the –4 power law for wind surface waves (Mitsuyasu, 1995), and thus the motion of sea surface waves affected the velocity fluctuation near the seabed. Moreover, the velocity spectra in Figure 8(c) shows that the inertial subranges of turbulence followed the –5/3 power law except for near the peaks. Therefore, the spectra in Figure 8(c) and Figure 5(a) have the similar characteristics.

Additionally, as shown in Figure 8(b), in Burst 4, the double logarithmic plot of $F_\eta(f)$ did not follow the –4 power law since the power of $F_\eta(f)$ was shifted from the equilibrium range of wind waves following the law to a low frequency range due to wave breaking. On the other hand, each velocity spectrum in Figure 8(b) is similar to the corresponding ones in Figure 8(c), and each inertial subrange of turbulence in Figure 8(b) is similar to that in Figure 8(c). Moreover, the spectra for Burst 3 (Figure 8(a)) are almost the same as those for Burst 5 (Figure 8(c)), except for the fact that the peaks of the spectra for Burst 3 are considerably smaller than those for Burst 5, because both Burst 3 and Burst 5 correspond to each maximum ebb tide in the spring tides.

Furthermore, the turbidity was greater in Bursts 4 and 5 compared with that in Burst 3 owing to the increased wave height and the wave breaking. The relationships among turbidity, mean flow velocity, wave height, and turbulence were examined. Turbidity, WL, V_{bm}, $H_{1/3}$, k, k^*, and dWL/dt were found to be 2.8 ppm, 8.27 m, 17.8 cm/s, 0.25 m, 3.06 cm^2/s^2, 2.39 cm^2/s^2, and –1.12 m/hr, respectively, in Burst 3; 23.2 ppm, 10.57 m, 10.9 cm/s, 0.89 m, 21.0 cm^2/s^2, 3.19 cm^2/s^2, and

0.11 m/hr, respectively, in Burst 4; and 31.7 ppm, 8.99 m, 18.0 cm/s, 0.61 m, 20.6 cm^2/s^2, 3.71 cm^2/s^2, and –0.97 m/hr, respectively, in Burst 5. That is, the turbidity in Burst 3 is relatively small even though the tidal current is relatively large because $|dWL/dt|$ is extremely large (see Figure 2(b)). On the other hand, the turbidity in Burst 5 is unusually large since the wave height, tidal current ($|dWL/dt|$ and V_{bm}) and turbulence are sufficiently large. However, the turbidity in Burst 4 is also large since not only waves but also turbulence due to wave breaking are remarkably large although the tidal current (dWL/dt) is quite small. It should be noted that the V_{bm} of 10.9 cm/s in Burst 4 is considerably large, which is mostly due to the large value of $\langle v \rangle$ of 10.8 cm/s, although Burst 4 is a high tide as WL is quite large. This eastward flow in Burst 4 is possibly the result of outflow discharge from the Isahaya sea-dyke or a mean flow related to features of wave breaking such as undertow.

6. CONCLUSIONS

Turbidity near the seabed at a transitional depth was found to be affected not only by sea surface waves but also spilling-type wave breaking. Long-term field observations were performed in Isahaya Bay in the Ariake Sea in order to determine the characteristics of SS in the neritic region in an inner bay involving waves at a transitional depth. In this study, turbidity was used as a proxy for SS, and two events where both turbidity and wave height were remarkably large were discussed in detail.

Spilling-type wave breaking was found to increase the turbulent kinetic energy where the turbulence intensity in the wave direction was markedly increased during an event (Event A) because the water depth was too large for shallow water waves to form, which means that waves occurred at a transitional depth. Therefore, the amplitude of the velocity spectrum in the wave direction became large at almost all frequencies, which was a kind of parallel translation in keeping with the –5/3 power law for the inertial subrange of turbulence. As a result, the anisotropy of turbulence removing the surface wave components was strengthened by the wave breaking.

The results of this study suggest that the effects of sea surface waves and wave breaking should be considered when estimating sedimentation in inner bays. The mean flow velocity near the seabed with spilling-type wave breaking during another event (Event B) was found to be remarkably large, although tidal current was notably weak due to the high tide.

ACKNOWLEDGMENTS

This study was funded in part by the Cooperative Monitoring Program of the Ariake Sea (COMPAS) of the Japanese Ministry of Education, Culture, Sports, Science and Technology.

REFERENCES

Goda, Y. (1981). Numerical Examination of the Measuring Technique of Wave Direction with the 'Covariance Method'. Report of the Port and Harbour Research Institute, Vol. 20, No. 3, pp.53-92 (in Japanese).

Goda, Y. (2008). Resistive Engineering against Wave Action -Structurally Resistive Design against Wave Action for Port and Coastal Structures-. Kajima Institute Publishing Co., Ltd., ISBN 978-4-306-02399-4 C3052, 430p. (in Japanese).

Li, H. and Matsunaga, N. (2010). Environmental Characteristics of Sediment in Isahaya Bay. *Journal Japan Society Civil Engineers*, Ser. B, Vol.66, No.4, pp.321-334 (in Japanese).

Mitsuyasu, H. (1995). Physics of Ocean Waves. Iwanami Shoten, Publishers, ISBN 4-00-005080-X, 210p. (in Japanese).

Nakagawa, Y., Imabayashi, S. and Suetsugu, K. (2002). Field Data Analysis for Muddy Sediment Transport Process in Ariake Bay. Proc. *Coastal Engineering*, JSCE, Vol. 49 (1), pp.566-570 (in Japanese).

Nakagawa, Y., Yoshida, H., Tanaka, K. and Ohhata, M. (2007). Field Survey on Resuspension of Fine Sediments and Turbulence Structures in a Bottom Boundary Layer. Annual Journal of *Coastal Engineering*, JSCE, Vol. 54 (1), pp.446-450 (in Japanese).

Nakagawa, Y., Ishinuki, K., Soeda, H. and Nakamura, Y. (2009). Field Observation of Sediment Transport Process off Shallow Coast with Tidal Flat. Journal of *Coastal Engineering*, JSCE, Vol. 56 (1), pp.471-475 (in Japanese).

Nakamura, T., Tada, A., Yano, S., Takeda, M. and Nonaka, H. (2003). Field Observation on Tidal Currents in Summer at Bay Mouth of Isahaya Bay. Proceedings of *Coastal Engineering*, JSCE, Vol. 50 (1), pp.371-375 (in Japanese).

Oshikawa, H., Yoshitake, R., Tai, A. and Hayami, Y. (2016). Behavior of Suspended Solids in the Neritic Region of an Inner Bay. Proc. 20th *IAHR-APD* Congress, 8p.

Tai, A., Tanaka, K. and Saita, T. (2013). Secular Change of Semidiurnal Tide in the Ariake Sea, Japan. Proc. *Global Congress on ICM*, pp.1198-1207.

Tai, A., Oba, T., Hayami, Y., Komatsu, T., Yano, S. and Tada, A. (2015). A Study on Flow Characteristics in the Isahaya Sea Based on Field Observations, *Journal of Japan Society of Civil Engineers*, Ser. B2 (Coastal Engineering), Vol.71, No.2, pp.433-438 (in Japanese).

Winterwerp, J. C., W. G. M. van Kesteren, B. van Prooijen and W. Jacobs (2012). A conceptual framework for shear-flow induced erosion of soft cohesive sediment beds. *Journal Geophysical Research*, Vol. 117, C10020, 17p.

Yano, S., Saita, T., Nishinokubi, H. and Komatsu, T. (2005). Impact of reclamation in Isahaya Bay on water environment in Ariake Sea, Japan. *Environmental Hydraulics and Sustainable Water Management*, Lee & Lam (Eds.), Taylor & Francis Group, London, Vol. 1, pp.1149-1154.